Title: Machine Learning Reveals the Contribution of Rare Genetic Variants and Enhances Risk Prediction for Coronary Artery Disease in the Japanese Population

Authors:

Hirotaka Ieki [1,2,3,4], Kaoru Ito [1*], Sai Zhang [5], Satoshi Koyama [1,6,7], Martin Kjellberg [3,8], Hiroki Yoshida[1,2], Ryo Kurosawa [1], Hiroshi Matsunaga [1,2], Kazuo Miyazawa [1], Nobuyuki Enzan [1,6,7], Changhoon Kim [9], Jeong-Sun Seo [9,10], Koichiro Higasa [11,12], Kouichi Ozaki[1,13], Yoshihiro Onouchi[1,14], The Biobank Japan Project, Koichi Matsuda [15], Yoichiro Kamatani [16], Chikashi Terao [17], Fumihiko Matsuda [12], Michael Snyder [3,4*], Issei Komuro [18,19*]

Affiliations:

[1] Laboratory for Cardiovascular Genomics and Informatics, RIKEN Center for Integrative Medical Sciences, Yokohama, Japan.

[2] Department of Cardiovascular Medicine, Graduate School of Medicine, The University of Tokyo, Tokyo, Japan.

[3] Department of Genetics, Center for Genomics and Personalized Medicine, Stanford University School of Medicine, Stanford, USA.

[4] Stanford Cardiovascular Institute, Stanford University School of Medicine, Stanford, USA.

[5] Department of Epidemiology, University of Florida, Gainesville, USA.

[6] Center for Genomic Medicine, Department of Medicine, Massachusetts General Hospital, Boston, MA, USA.

[7] Program in Medical and Population Genetics, Broad Institute of Harvard and MIT,

Cambridge, MA, USA.

[8] School of Engineering Sciences in Chemistry, Biotechnology and Health, Royal Institute of Technology (KTH), Stockholm, Sweden

[9] Bioinformatics Institute, Macrogen Inc., Seoul, Republic of Korea.

[10] Asian Genome Institute, Seoul National University Bundang Hospital, Gyeonggi-do, Republic of Korea.

[11] Department of Genome Analysis, Institute of Biomedical Science, Kansai Medical University, Hirakata, Japan.

[12] Human Disease Genomics, Center for Genomic Medicine, Kyoto University Graduate School of Medicine, Kyoto, Japan.

[13] Medical Genome Center, Research Institute, National Center for Geriatrics and Gerontology, Obu, Japan.

[14] Department of Public Health, Chiba University Graduate School of Medicine, Chiba, Japan.

[15] Department of Computational Biology and Medical Science, Graduate School of Frontier Sciences, The University of Tokyo, Tokyo, Japan.

[16] Laboratory of Complex Trait Genomics, Department of Computational Biology and Medical Sciences, Graduate School of Frontier Sciences, The University of Tokyo, Tokyo, Japan.

[17] Laboratory for Statistical and Translational Genetics, RIKEN Center for Integrative Medical Science, Yokohama, Japan

[18] International University of Health and Welfare, Tokyo, Japan

[19] Department of Frontier Cardiovascular Science, Graduate School of Medicine, The University of Tokyo, Tokyo, Japan

Correspondence:

kaoru.ito@riken.jp (K.I.)

mpsnyder@stanford.edu (M.S.)

komuro-tky@umin.ac.jp (I.K.)

Summary

Genome-wide association studies (GWASs) have advanced our understanding of coronary artery disease (CAD) genetics and enabled the development of polygenic risk scores (PRSs) for estimating genetic risk based on common variant burden. However, GWASs have limitations in analyzing rare variants due to insufficient statistical power, thereby constraining PRS performance. Here, we conducted whole genome sequencing of 1,752 Japanese CAD patients and 3,019 controls, applying a machine learning-based rare variant analytic framework. This approach identified 59 CAD-related genes, including known causal genes like *LDLR* and those not previously captured by GWASs. A rare variant-based risk score (RVS) derived from the framework significantly predicted CAD cases and cardiovascular mortality in an independent cohort. Notably, combining the RVS with traditional PRS improved CAD prediction compared to PRS alone (area under the curve, 0.66 vs 0.61; p=0.007). Our analyses reinforce the value of incorporating rare variant information, highlighting the potential for more comprehensive genetic assessment.

Keywords

Coronary artery disease; Rare variants; Genetic risk estimation; Polygenic risk score; Myocardial infarction; Genome-wide association study; Machine learning; BioBank Japan

Introduction

Despite advancements in treatments and medications, coronary artery disease (CAD), encompassing conditions such as angina pectoris and myocardial infarction (MI), remains a leading cause of death worldwide [1,2]. CAD etiology is complex, involving a multifaceted interplay between genetic predisposition and environmental determinants. Lifestyle factors including diet, smoking, and physical activity are well-established contributors to the onset and progression of CAD [3,4]. Additionally, conditions such as elevated low-density lipoprotein (LDL) cholesterol, hypertension, and glucose intolerance further exacerbate the risk profile [5]. The importance of genetic predisposition is also underscored by a European twin study, which estimated that genetic factors contributed to over 50% of CAD development [6,7]. Therefore, understanding the genetic underpinnings of CAD and accurately estimating an individual's lifetime genetic risk are crucial for effective prevention and management strategies.

To date, genome-wide association studies (GWASs) and their meta-analyses have identified more than 300 loci associated with CAD [8–12]. Polygenic risk scores (PRSs) derived from GWAS summary statistics have enabled the estimation of individual-level CAD risk [13,14]. However, despite these significant advancements, the heritability of CAD explained by GWASs remains lower than anticipated. This gap may be partly attributed to the primary focus of GWAS on low frequency to common variants, while rare variants are often underrepresented in these analyses [5,15]. Rare variants often have a large effect size on diseases and phenotypes, making them a promising target for drug development [16]. Incorporating rare variants into genetic risk scores could significantly enhance the accuracy of CAD prediction. Despite this

potential, previous GWASs and aggregated rare variant association analyses have struggled even in large-scale sequencing studies, identifying only a few genes at exome-wide significance per trait [17,18]. Furthermore, calculating a genetic risk score based on rare variants is challenging because gene-level effect sizes are not estimated by conventional gene-based analysis methods.

Recently, advancements in machine learning have led to the development of novel methods for genetic analysis, one of which is the HEAL (Hierarchical Estimate from Agnostic Learning) method, a machine learning-based framework for comprehensive rare variant analysis. This approach has been successful in identifying disease-associated genes and creating genetic risk scores in patients with abdominal aortic aneurysm [19]. In the current study, we conducted whole genome sequencing (WGS) of Japanese CAD patients and applied a modified version of the HEAL framework tailored for CAD to analyze rare variants and systematically prioritize disease-associated genes. Furthermore, we developed a rare variant-based genetic risk score (RVS) using this framework and validated the performance with an independent cohort. We then explored the relationship between the RVS and GWAS-based PRS to elucidate the characteristics of rare variants in CAD, bridging the gap in our understanding of CAD genetics by incorporating rare variant information, potentially uncovering novel insights into disease mechanisms and improving risk prediction models.

Results

Whole genome sequencing of CAD samples in the Japanese population

The overview and the design of our study are shown in **Figure 1**. We performed WGS on the discovery cohort comprising 1,765 Japanese CAD patients and 3,148 controls. In order to enhance the genetic discovery power [20], we prioritized patients with early-onset MI, a severe form of CAD, from the BioBank Japan (BBJ) cohort. The average age of MI onset in these patients was 47.4 ± 4.1 years, indicating a relatively young population with a severe disease phenotype. After quality control of the WGS data, we retained 4,771 individuals (1752 cases and 3019 controls) with 51,717,580 genetic variants. For the validation WGS cohort, we included 200 CAD cases and 824 control samples with 25,531,471 variants (**Table S1 and S2**). Demographic features in each cohort are summarized in **Table 1**. We then used the quality-controlled data for further analyses including single variant association tests to identify individual variants associated with CAD, a conventional gene-based association test to examine the cumulative effect of variants within specific genes, and a machine learning-based framework to uncover the potential contribution of rare variants (**Figure S1**).

We first conducted a single variant association test in the discovery cohort using a logistic regression model implemented in PLINK software with covariates of age, sex and top ten ancestry principal components (PCs). The genomic inflation factor λ_{GC} was calculated to be 1.03, indicating minimal inflation of test statistics and suggesting that the quality control applied to the samples was adequate (**Figure S2**). This initial single variant association analysis did not identify any genetic loci that reached a genome-wide significance threshold of $P = 5 * 10^{-8}$. A subsequent analysis

was performed using SAIGE software designed to handle both common and rare variants, adjusted for age, sex and top ten ancestry PCs. This analysis revealed two previously reported loci on chromosome 12 that reached a genome-wide significance threshold (rs7977233; $p=1.47 * 10^{-8}$, rs3782886; $p=1.47 * 10^{-8}$, respectively, (**Figure S3 and Table S3**))[10,11]. However, these were both common variants, emphasizing the difficulty in analyzing rare variants using current GWAS approaches.

To increase the detection power of rare variant associations, gene-based tests are often used, in which variants are aggregated and analyzed together for each gene. This approach allows for the analysis of rare variants that are underpowered in single variant association tests due to their low frequency. It also increases detection power by reducing the multiple testing burden. Thus, we conducted a gene-based rare variant aggregated association analysis using the sequential kernel association test-optimal (SKAT-O). While no genomic inflation was observed ($\lambda = 0.939$) (**Figure S4**), the *LDLR* gene surpassed a suggestive threshold ($p = 2.3\times10^{-5}$). However, no genes reached the gene-wide significance threshold of $p = 2.5\times10^{-6}$ (**Figure S4 and Table S4**). This result also highlighted the challenges of analyzing rare variants in genetic association studies due to insufficient statistical power with a limited sample size.

The machine learning-based framework prioritizes disease-associated genes and reveals molecular networks

We next conducted a machine learning-based rare variant analysis using a modified HEAL [19]. In this framework, we first quantified the mutation burden for each gene in each participant defined by the cumulative effects of deleterious nonsynonymous variants within the gene. We then trained a penalized logistic

regression model to predict disease status based on these mutation burden scores. The model was trained to identify a minimal set of most distinguishing features (genes) for CAD, while also optimizing parameters for accurate disease prediction. Through robust cross-validation (**Figure S5**), we successfully prioritized fifty-nine candidate genes associated with CAD development (**Table S5, S6 and Figure S6)**.

To investigate the functions of the fifty-nine $HEAL_{CAD}$ genes, we assessed constraint scores and checked for overlaps with neighboring genes identified in previous GWASs on CAD and its risk factors. Using the Genehancer database [21], which provides information on genome-wide enhancers and their target genes, we identified prioritized genes that overlapped with the target genes of enhancers found significant in previous GWASs. We also referenced the International Mouse Phenotyping Consortium (IMPC) [22] database to investigate the phenotypes associated with a gene knockout (KO) in mice and conducted gene set enrichment analysis to identify functional clusters among the $HEAL_{CAD}$ genes. The genes were subsequently categorized into eight distinct clusters based on the hierarchical clustering of their functional annotations (**Figure 2A, 2B and Table S7**).

Among these clusters, cluster 3 notably included the *LDLR* gene, which exhibited the strongest contribution to CAD. *LDLR* is a well-established causal gene for familial hypercholesterolemia [23] and has been consistently associated with CAD in previous GWASs and genome sequencing studies [9,24,25], supporting the validity of our machine learning-based framework. In the IMPC database, *LDLR* KO mice showed increased circulating cholesterol levels [26], a known risk factor for CAD. Cluster 7 contained genes related to obesity and metabolic processes, such as the *RNF216* locus, which is associated with body mass index (BMI) [27] and increased glucose levels in KO

mice [22]. Additionally, the *VRK2* locus has been reported to be associated with BMI [28], smoking behavior and alcohol use [29], indicating its broader impact on metabolic health. Cluster 2 comprised genes identified by previous GWAS on phenotypes such as blood pressure, diabetes, and cholesterol levels. The *FTO* gene within this cluster was highlighted for its strong association with obesity [30,31] and related phenotypes linked to BMI [32], LDL cholesterol [33], blood pressure [34], and CAD [35]. Cluster 8 encompassed genes associated with cholesterol levels, obesity and blood pressure in GWAS and GeneHancer categories, with phenotypic evidence in human and KO mice. For instance, the *CYP27A1* locus is associated with diastolic blood pressure [36] and triglyceride levels [37] and has connections to cholesterol levels and premature CAD according to human phenotype ontology [38].

To further determine the functions of the fifty-nine genes, we mapped them onto the human protein-protein interaction (PPI) network followed by identifying proteins that were tightly clustered with these $HEAL_{CAD}$ genes as topological modules [19]. We identified 46 tightly clustered topological modules encompassing the $HEAL_{CAD}$ genes. Gene ontology analysis confirmed the functional coherence of the proteins within each module, revealing significant enrichment for specific biological processes. For instance, module M119 was significantly enriched for lipid homeostasis with a false discovery rate (FDR) of $2.53*10^{-22}$, suggesting a critical role in regulating lipid levels (**Figure 2C and Table S8**). These modules included pathways known as CAD risk factors, such as lipid and glucose metabolism (M25, M31, M51, M86, M119). Notably, M119 included lipid metabolism-related genes such as *LDLR*, *PCSK9*, *LIPA*, and *ANGPTL3* (**Figure 2D**), which are well-known targets for medications treating dyslipidemia and CAD [39 40]. Other modules were associated with different biological

219 processes, including platelet volume (e.g., M13), immune system function (M1), blood
220 vessel and heart development (e.g., M47, M328), and RNA metabolism and translation
221 processes (e.g., M3, M34). While recent studies have indicated the contribution of
222 common variants identified by CAD-GWAS to the disease through various pathways
223 such as plaque formation, inflammation, transcriptional regulation, and angiogenesis [41],
224 our findings suggest that diverse biological processes are also implicated in CAD, even
225 in the context of rare variants. This underscores the complexity of CAD pathogenesis,
226 involving a wide array of biological pathways and molecular mechanisms.
227
228 **Rare variant risk-based risk score and its clinical impact**
229 In conjunction with the prioritization of disease-related genes, the modified
230 HEAL enabled us to develop a prediction model for CAD based on genetic information.
231 Using the optimized machine learning model, we computed a rare variant-based risk
232 score (RVS) for each individual. The RVS demonstrated a significant predictive
233 capability for CAD, with an area under the receiver operating characteristics curve
234 (AUROC) of 0.574, as validated through a nested cross-validation approach in the
235 discovery cohort. When applied to an independent validation cohort, the RVS also
236 identified CAD cases with an AUROC of 0.581 ($p = 0.002$), indicating its ability to
237 discriminate CAD cases.
238 To further understand the characteristics of RVS in terms of clinical aspects,
239 we explored the association of RVS with clinically relevant parameters. The RVS
240 showed significant correlations with several key clinical measurements, including low-
241 density-lipoprotein cholesterol (LDLC), total bilirubin (TBil), alanine aminotransferase
242 (ALT), prothrombin time (PT-INR), total cholesterol levels, neutrophil count, and

243 potassium levels (**Figure 3A and Table S9**). These correlations are noteworthy since
244 elevated cholesterol levels and coagulation abnormalities are established risk factors for
245 CAD [42–44]. Moreover, alterations of total bilirubin and AST were also reported to be
246 associated with cardiovascular risk [45,46], reinforcing the clinical relevance of the RVS in
247 the context of CAD.

248 We extended our analysis to assess the impact of the RVS on long-term
249 cardiovascular mortality. In the validation cohort, a higher RVS was significantly
250 associated with increased cardiovascular mortality (P = 0.01, log-rank test) (**Figure 3B)**.
251 When exclusively analyzing CAD patients, those with higher RVS also exhibited a
252 significantly worse cardiovascular mortality rate (p = 0.03, log-rank test) (**Figure 3C**).
253 These findings suggest that RVS not only predicts CAD occurrence but also correlates
254 with the disease severity and its long-term prognosis, highlighting its potential clinical
255 utility in risk stratification and prognosis estimation for CAD patients.

256

257 **The integration of RVS and PRS improves the performance of the genomic risk**
258 **score**

259 Many GWASs have been conducted for CAD, leading to the development of
260 PRS that primarily comprise common variants to predict the risk of CAD. Multiple
261 studies have reported that PRS can serve as an important indicator for predicting and
262 assessing the severity of CAD. Whereas these scores typically focus on common
263 variants and do not account for rare variants, which can also significantly contribute to
264 disease risk, our RVS encompasses rare variants not included in PRS. Thus, to compare
265 the properties between RVS and PRS, we first calculated individual PRS based on
266 CAD-GWAS [11] in the validation cohort. The PRS also significantly predicted CAD with

an AUROC of 0.61 (p = 0.001; 95% confidence interval (C.I.), 0.565-0.653). Interestingly, there was no significant correlation between PRS and RVS (r = -0.01, p = 0.73) (**Figure 4A**), indicating that RVS provides a different genomic perspective on CAD risk.

When examining CAD cases specifically, RVS showed a negative correlation with PRS (r = -0.17, p = 0.015) (**Figure 4A**). Additionally, PRS was associated with different clinical measurements compared to RVS, such as triglycerides, uric acid, body mass index (BMI), and activated partial thromboplastin time (APTT) and it was negatively associated with HDL cholesterol (HDLC), which is considered protective against CAD (**Figure 3A, Figure S7 and Table S10**) [47]. These data support the notion that PRS and RVS may have complementary rather than redundant roles in predicting CAD, as they were associated with different clinical parameters and did not show a positive correlation.

Given these distinct properties, we integrated PRS and RVS to develop a combined risk score (CRS) aiming at enhancement of the performance of the framework in predicting CAD. The CRS showed positive correlations with several clinical measures, including serum urinary acid, coagulation functions, LDLC, and triglycerides (TG), while negatively correlating with HDLC levels (**Figure 4B and Table S11**). Focusing on lipid metrics, CRS demonstrated correlations with LDLC, TC, TG, and HDLC, suggesting that it combines the unique predictive elements of both RVS and PRS (**Figure 4C**). Finally, we evaluated the predictive performance of CRS and observed a significant improvement in CAD prediction compared to PRS alone in the validation cohort (AUROC 0.66 vs 0.61, p=0.007; Pseudo R^2 0.093 vs 0.040, p = 0.0018; AUPRC 0.35 vs 0.29, p = 0.0154) (**Figure 5 and Table S12**). These results

suggest that RVS can complement PRS and that incorporating rare variant information as an RVS into PRS significantly enhances the ability to predict CAD, thereby addressing some of the unexplained heritability in the disease.

Discussion

In this study, we developed a machine learning-based analytical framework to investigate the genetics of CAD pathogenesis with a focus on rare variants. We leveraged this framework together with whole-genome sequencing (WGS) data from the Japanese population to enhance our understanding of the complex CAD genetic architecture. Our findings indicated that the modified HEAL, a machine learning-based framework, effectively prioritized genes associated with CAD, including the well-established *LDLR* gene, while also uncovering intricate molecular networks involved in the disease. The rare variant-based risk score (RVS) generated through this framework demonstrated significant predictive power for CAD and long-term cardiovascular mortality Furthermore, the RVS showed different characteristics from conventional common variant-based PRS, and combining the rare variant-based RVS with the PRS substantially improved CAD prediction.

Identifying disease-associated rare variants remains a significant challenge, not only in single variant association analyses but also in aggregated rare variant association analyses [48,49]. While some studies have adopted a targeted resequencing approach by selecting specific genes based on prior knowledge [25,50]; previous attempts at genome-wide or exome-wide analyses have often suffered from insufficient statistical power, leading to limited success in identifying previously uncharacterized genes associated with complex traits like CAD [20]. Also in this study, the single variant association analysis and the gene-based rare variant association analysis failed to reveal genome-wide significant rare variants linked to CAD. Even in previous studies involving more than 450,000 exome sequencing data from the UK biobank, only a single gene, *LDLR*, reached a significance level in the gene-based test for CAD [17].

These persistent challenges highlight the difficulties in rare variant analyses.

To address these challenges, we utilized a machine learning-based framework to analyze rare variants, building on the HEAL model in a prior study, where Li et al. successfully uncovered the genetic architecture of rare variants in abdominal aortic aneurysm [19]. We adapted and optimized the model for CAD patients, marking the first application of the technique in this disease context. Unlike the previous HEAL model that focused only on missense single nucleotide variants (SNVs), our approach casts a wider net as it incorporates insertion, deletion and putative loss-of-function (pLOF) variants. This comprehensive inclusion of variant types allows for a more holistic examination of the genetic landscape underlying CAD, potentially capturing a broader spectrum of disease-associated genetic alterations. Furthermore, the robustness of our model was enhanced by hyperparameter tuning through a grid search to avoid overfitting and we evaluated its predictive performance using both internal cross-validation and an independent validation cohort [51].

Through this improved framework, we successfully prioritized CAD-associated genes, extending beyond previously reported genes such as *LDLR*, *FTO*, and *CYP27A1*. By mapping these genes onto the human protein-protein interaction network, we uncovered 46 tightly clustered topological modules, providing insights into their functional roles in CAD pathogenesis. Beyond lipid metabolism, the analysis revealed modules associated with other relevant biological processes, including platelet function, immune system regulation, blood vessel and heart development, and RNA metabolism. Interestingly, while previous GWASs have highlighted the role of common variants in CAD development through various pathways, our findings suggest that rare variants also contribute to the disease through a wide spectrum of biological processes.

We also utilized our framework to develop an RVS and demonstrated its discriminative capacity between CAD cases and controls in the validation cohort. The distinctive feature of RVS lies in its utilization of rare nonsynonymous variants as input data, setting it apart from conventional PRS that primarily focus on common variants. This approach allows RVS to tap into a different spectrum of genomic information, involving risk factors uncaptured by PRS. The independence of RVS from PRS is further substantiated by the absence of a significant positive correlation between these two scoring systems and the complementary relationships with clinical risk parameters. This lack of correlation suggests that the RVS and PRS are capturing distinct aspects of genetic risk for CAD, each contributing unique information to the overall risk assessment. Importantly, the integration of RVS and PRS resulted in improved predictive performance, demonstrating a synergistic effect that enhanced the ability to accurately assess CAD risk. While methods combining information from one or a few genetic mutations with PRS have been reported [52], our study presented a more comprehensive approach to combine rare and common variant information. Furthermore, these findings reinforce the recognition that rare variants, despite their low frequency, contribute significantly to the genetic architecture of CAD and can help explain a portion of its missing heritability that common variants alone cannot account for.

There are several limitations in the study. First, there was a difference in age distribution between cases and controls. This discrepancy arose because we specifically selected early-onset CAD patients for the case group, resulting in a younger average age. As in previous rare variant studies, we prioritized selecting early-onset CAD cases to enrich genetic contributions [20]. Second, some of the prioritized genes for CAD in this

study have unknown functions, especially in cluster 6. However, many loci and genes identified in GWAS on CAD remain functionally uncharacterized, as well [41,53]. Therefore, future research is necessary to investigate the gene function and biological pathways to CAD development. Third, this study used WGS data from the Japanese population, so it is not certain whether the RVS created in this study can be applied to other populations since a PRS derived from GWAS in one population is reported to be less accurate in other populations [11,54]. These results need to be validated in other populations and prospective cohorts.

Taken together, our study underscores the important role of rare variants in the genetic landscape of CAD. By leveraging a machine learning-based framework, we have revealed CAD-associated genes and pathways influenced by rare variants. Our results demonstrate the distinct and complementary value of RVS compared to conventional PRS, highlighting the enhanced predictive power achieved through their integration. This comprehensive approach offers new insights into the pathogenesis of CAD, potentially leading to the accurate assessment and management of individual CAD risk.

Consortia

The Biobank Japan Project

Koichi Matsuda[1,2], Takayuki Morisaki[2,3], Yukinori Okada[4], Yoichiro Kamatani[5], Kaori Muto[6], Akiko Nagai[6], Yoji Sagiya[2], Natsuhiko Kumasaka[7], Yoichi Furukawa[8], Yuji Yamanashi[3], Yoshinori Murakami[3], Yusuke Nakamura[3], Wataru Obara[9], Ken Yamaji[10], Kazuhisa Takahashi[11], Satoshi Asai[12,13], Yasuo Takahashi[13], Shinichi Higashiue[14], Shuzo Kobayashi[14], Hiroki Yamaguchi[15], Yasunobu Nagata[15], Satoshi Wakita[15], Chikako Nito[16], Yu-ki Iwasaki[17], Shigeo Murayama[18], Kozo Yoshimori[19], Yoshio Miki[20], Daisuke Obata[21], Masahiko Higashiyama[22], Akihide Masumoto[23], Yoshinobu Koga[23] & Yukihiro Koretsune[24]

[1.] Laboratory of Genome Technology, Human Genome Center, Institute of Medical Science, The University of Tokyo, Tokyo, Japan.

[2] Laboratory of Clinical Genome Sequencing, Graduate School of Frontier Sciences, The University of Tokyo, Tokyo, Japan.

[3] The Institute of Medical Science, The University of Tokyo, Tokyo, Japan.

[4] Department of Genome Informatics, Graduate School of Medicine, The University of Tokyo, Tokyo, Japan.

[5] Laboratory of Complex Trait Genomics, Graduate School of Frontier Sciences, The University of Tokyo, Tokyo, Japan.

[6] Department of Public Policy, Institute of Medical Science, The University of Tokyo, Tokyo, Japan.

[7] Division of Digital Genomics, Institute of Medical Science, The University of Tokyo, Tokyo, Japan.

[8] Division of Clinical Genome Research, Institute of Medical Science, The University of Tokyo, Tokyo, Japan.

[9] Department of Urology, Iwate Medical University, Iwate, Japan.

[10] Department of Internal Medicine and Rheumatology, Juntendo University Graduate School of Medicine, Tokyo, Japan.

[11] Department of Respiratory Medicine, Juntendo University Graduate School of Medicine, Tokyo, Japan.

[12] Division of Pharmacology, Department of Biomedical Science, Nihon University School of Medicine, Tokyo, Japan.

[13] Division of Genomic Epidemiology and Clinical Trials, Clinical Trials Research Center, Nihon University. School of Medicine, Tokyo, Japan.

[14] Tokushukai Group, Tokyo, Japan.

[15] Department of Hematology, Nippon Medical School, Tokyo, Japan.

[16] Laboratory for Clinical Research, Collaborative Research Center, Nippon Medical School, Tokyo, Japan.

[17] Department of Cardiovascular Medicine, Nippon Medical School, Tokyo, Japan.

[18] Tokyo Metropolitan Geriatric Hospital and Institute of Gerontology, Tokyo, Japan.

[19] Fukujuji Hospital, Japan Anti-Tuberculosis Association, Tokyo, Japan.

[20] The Cancer Institute Hospital of the Japanese Foundation for Cancer Research, Tokyo, Japan.

[21] Center for Clinical Research and Advanced Medicine, Shiga University of Medical Science, Shiga, Japan.

[22] Department of General Thoracic Surgery, Osaka International Cancer Institute, Osaka, Japan.

[23] Iizuka Hospital, Fukuoka, Japan.

[24] National Hospital Organization Osaka National Hospital, Osaka, Japan.

Acknowledgements

We thank the staff of BBJ and the Nagahama cohort study for their assistance in collecting samples and clinical information. We thank the participants in the BBJ and Nagahama cohort study for their contribution to the study. H.I. is funded by the Japan Society for the Promotion of Science grant (JP22J00780, JP22K16128). K.I. is supported by the Japan Agency for Medical Research and Development (AMED) under grant numbers JP24bm1423005, JP24km0405209, JP24tm0524004, JP24tm0624002, JP24km0405209 and JP24ek0210164. K.I. and K.O. are supported by the Research Funding for Longevity Sciences from the NCGG (24–15). BBJ is supported by the Tailor-Made Medical Treatment Program of the Ministry of Education, Culture, Sports, Science, and Technology (MEXT) and AMED under grant numbers JP17km0305002 and JP17km0305001, JP.24tm0624002. The Nagahama study was supported by a JSPS Grant-in-Aid for Scientific Research (C), KAKENHI grant numbers JP17K07255 and JP17KT0125, and the Practical Research Project for Rare/Intractable Diseases from AMED under grant numbers JP16ek0109070, JP18kk0205008, JP18kk0205001, JP19ek0109283, and JP19ek0109348.

Author contributions

H.I. and K.I. conceived and designed the study. C.K., J.S., K.H., and F.M. collected, managed and genotyped the Nagahama cohort. K.M., C.T. and Y.K. collected and managed the BBJ samples. H.I. and K.I. analyzed WGS data, developed the

457 machine-learning model and performed the statistical analyses. S. K estimated the effect
458 size to calculate PRS. S.Z. developed the PPI network module and analyzed it. H.Y.,
459 R.K., H.M., K.M., N.E., K.O., Y.O., C.T., and Y.K. contributed to data processing,
460 analysis and interpretation. K.I., M.S. and I.K. supervised the study. H.I. and K.I. wrote
461 the manuscript, and many authors have provided valuable insights and edits.
462
463 **Declaration of Interests**
464 H.I. reports receiving grants from the Japan Heart Foundation / Bayer
465 Pharmaceutical Research Grant Abroad. M.S. is a co-founder and the scientific advisory
466 board member of Personalis, Qbio, January, SensOmics, Filtricine, Akna, Protos, Mirvie,
467 NiMo, Onza, Oralome, Marble Therapeutics, and Iollo. He is also on the scientific
468 advisory board of Danaher, Genapsys and Jupiter.
469
470 **Supplemental information**
471 **Document S1.** Table S1-S3, S5, S7, S9-13, Figure S1-8
472 **Table S4.** Summary statistics of aggregated rare variant association analysis using
473 SAIGE-GENE+, related to Figure S4.
474 **Table S6.** Summary of 59 $HEAL_{CAD}$ genes with gene-based annotation, related to
475 Figure 2.
476 **Table S8.** The 46 Protein Interaction Modules Identified in CAD, Related to Figure 2.
477
478

Figure legends

Figure 1. Overview of the current study.

We studied the genetic factors of coronary artery disease (CAD) combining whole-genome sequencing data and a machine learning-based framework named the modified HEAL method in patients with MI, one of the most severe forms of CAD, and controls. We sequenced the whole genomes of Japanese CAD patients and controls and applied the modified HEAL method framework. The framework was based on a sparse modeling devised to distinguish diseased individuals from controls. After the hyperparameter tuning and training of the model by the cross-validation method, the model outputted a list of genes related to CAD, which were subsequently analyzed by a clustering-based method and mapped on the protein-protein interaction network to reveal the CAD-associated modules. The function of the identified genes was also confirmed by the human phenotype and knockout mouse phenotype databases. The learned (optimized) machine learning model was applied to derive rare variant-based genetic risk scores (RVS) to predict CAD outcomes in an independent validation cohort. We also tested the relationship of the RVS with clinical features and common variant-based polygenic risk score (PRS). RVS was combined with PRS to improve the prediction performance of CAD disease status in the independent validation cohort. BBJ, BioBank Japan; MI, myocardial infarction; CRS, combined risk score

Figure 2. Functional analysis of $HEAL_{CAD}$ genes

(A) Fifty-nine genes identified by the machine learning-based framework were annotated using six different criteria; 1) The constraint score (pLI) from the gnomAD database 2) Overlap with GWAS on CAD and its risk factor (lipids, diabetes, obesity, blood pressure, coagulation, smoking) phenotypes, 3) Overlap with the genes in which GWAS-significant variants act as enhancers, 4) Knock-out mouse phenotype with blood pressure, diabetes, and lipid traits, 5) Human phenotype ontology and 6) Gene ontology. Then the fifty-nine genes were grouped into eight clusters by hierarchical clustering based on functional annotations. For GWAS and Genehancer, red indicates a significant association and light red denotes suggestive significance. (B) Gene ontology (GO) and human phenotype ontology (HPO) term enrichment analysis. The GO and HPO annotation results were based on 59 genes. Gene ontology categories included molecular function, cellular components and biological process. GO and HPO categories for each function were sorted by decreasing order of evidence based on the GO enrichment test P-value. Only the significant categories after multiple test corrections are shown. (C) The forty-six modules were identified in the protein-protein-interaction network using diffusion component analysis seeded by the 59 $HEAL_{CAD}$ genes. (D) Visualization of the module 119 network of the protein-protein interactions. The module included important genes involved in cholesterol metabolism, including *LDLR*, *PCSK9*, *ANGPTL3*, *ANGPTL4*, and *LIPA*. GWAS, genome-wide association study; CAD, coronary artery disease; DM, diabetes mellitus; BP, blood pressure; IMPC, International Mouse Phenotyping Consortium; HP, human phenotype; GOMF, gene ontology molecular function; GOBP, gene ontology biological pathway; GOCC, gene ontology cellular component.

524

Figure 3. Rare variant risk score (RVS) and its clinical impact

(A) Correlation between RVS and continuous clinical indices. Data are presented as Pearson's correlation coefficients and their 95% confidence intervals (CIs). Exact P values are shown in Table S9. (B) Kaplan-Meier curves for cardiovascular mortality among total participants stratified into two groups based on RVS. Participants with high RVS died significantly earlier than those with low RVS. (C) Kaplan-Meier curves for cardiovascular mortality among CAD patients (n=200) stratified into two groups based on RVS. CAD patients with high RVS (top 5%) showed significantly worse cardiovascular prognosis. LDLC, low-density lipoprotein cholesterol; Tbil, total bilirubin; ALT, alanine aminotransferase; PTINR, prothrombin time international normalized ratio; TC, total cholesterol; K, potassium; Hb, hemoglobin; UA, uric acid; APTT, activated partial thromboplastin time; Alb, albumin; RBC, red blood cell; AST, aspartate aminotransferase; WBC, white blood cell; CK, creatine kinase; TP, total protein; Cre, creatinine; DBP, diastolic blood pressure; SBP, systolic blood pressure; BUN, blood urea nitrogen; TG, triglycerides; CRP, C-reactive protein; PLT, platelet; P, Phosphorus; γGTP, gamma-glutamyl transpeptidase; BS, blood sugar; LDH, Lactate dehydrogenase.

Figure 4. The Relationship between RVS, PRS, CRS, and clinical indices.

(A) A scatter plot illustrating the relationship between RVS and PRS, with cases (red) and controls (gray) color-coded. The overall (gray) and case-only (pink) regression lines and correlation coefficients are shown. A significant negative correlation was observed in the CAD cases. (B) Correlation between combined risk score (CRS), defined by the average of RVS and PRS, and continuous clinical indices. Data are presented as Pearson's correlation coefficients and their 95% CIs. Exact P values are shown in Table S11. (C) Correlation between clinical measurements and different genetic risk scores (RVS, PRS and CRS). Only significant correlations are displayed with a circle. Blue, positive correlation; red, negative correlation. Larger circles correspond to a stronger correlation. LDLC, low density lipoprotein cholesterol; Tbil, total bilirubin; ALT, alanine aminotransferase; PTINR, prothrombin time international normalized ratio; TC, total cholesterol; K, potassium; Hb, hemoglobin; UA, uric acid; APTT, activated partial thromboplastin time; Alb, albumin; RBC, red blood cell; AST, aspartate aminotransferase; WBC, white blood cell; CK, creatine kinase; TP, total protein; Cre, creatinine; DBP, diastolic blood pressure; SBP, systolic blood pressure; BUN, blood urea nitrogen; TG, triglycerides; CRP, C-reactive protein; PLT, platelet; P, Phosphorus; γGTP, gamma-glutamyl transpeptidase; BS, blood sugar; LDH, Lactate dehydrogenase

Figure 5. The combined RVS and PRS risk score improved CAD prediction

(A) Receiver operating characteristic (ROC) curve for RVS, PRS and CRS (Combined Risk Score). The curve plots the true positive rate (sensitivity) against the false positive rate (1-specificity) for different threshold values of the predictive score. The area under the curve (AUC) is indicated, representing the score's accuracy in predicting the outcome. The dotted line represents a reference line of no discrimination (AUC = 0.5). Points on the curve closer to the top-left corner indicate higher diagnostic accuracy. (B) Precision-recall curve (PRC) for RVS, PRS and CRS. The curve shows the trade-off between precision (positive predictive value) and recall (sensitivity) at various threshold levels. The confidence interval for the area under the PRC was estimated from the 20,000 times bootstrap replication method. (C) Boxplot of Pseudo R^2 for CAD prediction performance. This box plot displays the pseudo-R^2 values comparing the CAD prediction performance of RVS, PRS and CRS. The distribution of pseudo-R^2 was estimated from 20,000 times bootstrapping. The box plot center line represents the median, the bounds represent the first and third quartile, and the whiskers reach to 1.5 times the interquartile range.

Tables

Table 1. Demographic features of participants

Data	Disease status	Total N	Males		Age (years)		BMI (kg/m^2)		Age at MI onset (years)	
			N	%	Mean	SD	Mean	SD	Mean	SD
Discovery cohort	Case	1,752	1,617	92.29	60.1	13.7	25.0	3.4	47.4	4.1
	Control	3,019	1,205	39.91	55.3	8.0	23.9	4.0	-	-
Validation cohort	Case	200	183	91.50	43.8	9.8	26.5	4.3	36.0	3.9
	Control	824	420	50.97	49.3	13.0	22.9	3.8	-	-

SD, standard deviation; BMI, body mass index; MI, myocardial infarction

STAR Methods

Code availability

The code of the modified HEAL framework is available on https://github.com/pirocv/HEAL.

Study cohort

Two previously described cohorts were used in the current study. BioBank Japan (BBJ) is a hospital-based Japanese biobank project including clinical and genetic data from a variety of patients [55,56]. Participants were recruited from 12 hospitals throughout Japan. The Nagahama Prospective Genome Cohort (Nagahama study) is the genome cohort conducted in Shiga, Japan. Participants aged 30–74 years were recruited from the general population in Nagahama city from 2007 to 2010 [57].

Whole genome sequencing and quality control

We sequenced 1,765 CAD patients and 3,148 controls from the cohort. Whole genome sequence (WGS) was performed on Illumina's HiSeqX aiming at 15x depth, using 150-base pair-end reads. We also sequenced an additional 200 CAD cases and 836 controls aiming at 30x depth using 150-base paired-end reads. In order to enrich for a genetic contribution to disease [20], we prioritized patients with early-onset MI, one of the most severe forms of CAD, within the BBJ cohort for WGS (age of MI onset in 15x and 30x WGS cohort: 47.4 ± 4.1 years and 36.0 ± 3.9 years, respectively). Sequenced reads were aligned to the hs37d5 reference genome using BWA software [58]. The genotypes of the samples were called using the HaplotypeCaller implemented in GATK v3.8. Per-sample Genomic Variant Call Format (gVCF) genotype data were merged and jointly called using GenotypeGVCFs. We defined exclusion filters for genotypes as follows.

(1) For 15x depth data, filtered depth (DP) < 2, quality of the assigned genotype (genotype quality; GQ) < 20. (2) For 30x depth data, DP < 5, GQ < 20, DP > 60 and GQ < 95. We set these genotypes as missing and excluded variants with call rates < 90% before variant quality score recalibration. For sample quality control, the following samples were excluded: (1) age < 20 years old, (2) excess missing genotypes (> 10%), (3) samples whose genetically inferred sex did not match the self-reported sex, (4) closely related samples estimated by identity-by-descent and identity-by-state analysis (Pi-hat > 0.1875) and (5) excess heterozygosity. We also excluded non-Japanese participants estimated from Principal component analysis (PCA) calculated using PLINK 2.0 [59]. The total number of genomes that failed data quality control is summarized in **Table S13**. After the sample quality control, we retained 1,752 CAD case samples and 3019 non-CAD control samples for 15x depth data and 200 case samples and 824 control samples for 30x depth. Then, the variant quality control was performed excluding (1) high missingness (5% for 15x depth and 1% for 30x depth), (2) Hardy-Weinberg equilibrium ($P < 1 * 10^{-6}$), (3) variants in the low complexity region. WGS data with 15x depth data was used as a discovery cohort and the 30x depth data was used as the validation cohort in the machine learning-based analysis.

Single variant association analysis

The single variant association test was performed by logistic regression implemented in PLINK 2.0 [60] with adjustment for age, sex, and the first 10 principal components of ancestry. Principal components of ancestry were calculated using PLINK 2.0 [59]. The inclusion of principal components as covariates in the logistic regression analysis increases the power to detect true genetic associations and minimizes

confounding by population stratification [61]. Variants with a missing rate of less than 0.01 were included in the analysis. Genomic inflation factor (λ_{GC}) was calculated using variants with MAF ≥ 0.001. Single variant association analysis was also performed using SAIGE [62] with adjustment for age, sex, and the first 10 principal components of ancestry. SAIGE is widely used in GWASs for binary traits to account for population structure and relatedness while correcting for the type I error rates [62]. The genome-wide significance threshold was set at $P = 5 * 10^{-8}$. To define a locus, we added 500 kb to both sides of each genome-wide significant SNP and merged overlapping regions. To determine whether each locus was novel, a literature search was conducted to ascertain if any of the regions contained SNPs had been previously reported as significant for CAD.

Aggregated rare variant association analysis

We also performed gene-based association analysis using SAIGE-GENE+ software, which accounts for the relatedness among the study samples [63,64]. We first calculated sparse GRM using the WGS data and fit the null model in the SAIGE-GENE+ algorithm step1. For the gene-based association analysis, we extracted rare (MAF < 0.001) nonsynonymous variants including (nonsynonymous single nucleotide variations (SNV), nonframeshift insertion, nonframeshift deletion, frameshift insertion, frameshift deletion, stopgain, stoploss, and splice site variants). Splice-site variants, pLOF variants and damaging missense variants defined by a REVEL score > 0.5 [65] were included in the analysis. SKAT-O test implemented in SAIGE-GENE+ software was performed with adjustment for age, sex and first 10 principal components of ancestry. Gene-wide significance threshold and suggestive threshold were set at $P = 2.5 * 10^{-6}$

and $P = 5 * 10^{-4}$, respectively. Statistical inflation was estimated by Q-Q plot.

Machine learning-based analysis (modified HEAL)

We employed a recently developed machine learning-based rare variant analysis method called HEAL (hierarchical estimate from agnostic learning). A detailed HEAL method is described in the original paper [19]. In this framework (**Figure S8**), we first annotated each variant using ANNOVAR software [66] and extracted rare nonsynonymous variants (nonsynonymous SNV, nonframeshift insertion, nonframeshift deletion, frameshift insertion, frameshift deletion, stopgain, stoploss, and splice site variants) that were not present in the East-Asian populations analyzed in the 1000 Genomes Project [67]. Variants with high frequency in the WGS data and gnomAD East Asian database [68] (MAF > 0.1) were also filtered. To estimate the mutation burden for each gene based on the rare variants, we used the REVEL score (ranges from 0 to 1 with a higher score indicating a damaging variant), which was internally computed by ANNOVAR software. The deleteriousness score of the putative loss of function (pLOF) variants, such as stopgain and splice site variants, was set as 1. Next, we calculated the cumulative effects of rare nonsynonymous variants for each gene as

$$g_{in} = \sum_{j=1}^{m_{in}} s_{ijn}$$

, where g_{in} is the mutation burden of the gene *i* of *n*th sample, m_{in} is the number of rare nonsynonymous variants, s_{ijn} is the deleteriousness score for variant *j* of gene *i*. Using the above formula, we obtained a matrix of estimated mutation burden for each gene per sample ($\boldsymbol{x_n} = (g_{1n}, g_{2n}, \ldots, g_{mn})$, where m is the number of the total genes). The mutation burden was standardized (Z-score normalization). We trained a regularized

677 logistic regression model for a genome-based CAD prediction model. The input of the
678 model is the calculated mutation burden and the output is the probability of CAD as
679 shown in the following equation.

$$\widehat{y_n} = P(y_n = 1|\boldsymbol{x_n}) = \sigma(\boldsymbol{w}^T\boldsymbol{x_n}) = \frac{1}{1 + exp(-w^T\boldsymbol{x_n})}$$

680 , where y_n is the label for CAD case (1) or control (0), $\widehat{y_n}$ is the probability of being
681 CAD positive given the mutation burden $\boldsymbol{x_n}$ for the *n*th sample, σ is the sigmoid
682 function and $\boldsymbol{w}$ is the weight vector. To identify the optimal coefficient vector $\boldsymbol{w}$ that
683 achieve the maximum consistency between the model probabilities ($\widehat{y_n}$) and the
684 observations for the cohort (y_n), we solved the following optimization problem.

$$\min_{\boldsymbol{w}} -\frac{1}{N}\sum_{n=1}^{N} y_n \, log\, \widehat{y_n} + (1 - y_n)\, log(1 - \widehat{y_n}) + \lambda\left|\left|\boldsymbol{w}\right|\right|_1$$

685 In this regularized logistic regression, regularization strength is determined by
686 parameter λ, and it is a hyperparameter of the machine learning model, which was
687 determined by the cross-validation method (**Figure S5**). By training the model to
688 predict disease status, it outputs the minimal set of most distinguishing features (genes)
689 for CAD. The trained model can be used to estimate the rare variant-based disease risk
690 score (RVS) from the genomic data. We have named this the modified HEAL because
691 our approach differs from the original method in that we included not only missense
692 variants but also pLOF variants. We determined the hyperparameters using grid search
693 and estimated the performance in the independent cohort to avoid bias and
694 overestimation of the model's performance, while the performance was estimated using
695 internal cross-validation in the original method.
696

Interpretation of genes identified by modified HEAL

To investigate the functions of the 59 identified genes, we first annotated each one using various databases and then conducted clustering analysis to categorize the groups of genes to obtain the eight functional groups. Annotations included checking the constraint score (pLI) from the gnomAD database [68], identifying whether the genes were reported in previous GWAS on CAD and its risk factors (lipids, diabetes, obesity, blood pressure, coagulation function, and smoking-related phenotypes) using the GWAS Catalog, and checking for the overlap with target genes of enhancers that were significant in previous GWAS on CAD and its risk factors (same as above) using the GeneHancer database, which includes genome-wide enhancers and their target genes [21]. Further analysis involved examining the International Mouse Phenotyping Consortium (IMPC) database to determine if the corresponding genes in knock-out mice are significantly related to phenotypes such as blood pressure, blood glucose and lipid traits. Enrichment analysis for Gene Ontology and Human Phenotype Ontology was performed using g:Profiler [69] to gain insights into the biological processes and human phenotypic abnormalities associated with these genes [22]. We considered statistical significance for the enrichment analysis with a false discovery rate under 0.1.

To analyze the functional modules in CAD, we downloaded the human protein-protein interactions (PPIs) from STRING v12.0, comprising 19,622 proteins and 6,857,702 interactions. High-confidence PPIs (combined score >700) were extracted for downstream analysis, including 16,185 proteins and 236,000 interactions. To remove bias from hub proteins, we applied the random walk with restart (RWR) algorithm with a restart probability of 0.5. This produced a smoothed network after retaining the top 5% predicted edges (n = 6,243,766). We employed the Louvain method [70] to decompose

the network into different modules. Following algorithm convergence, we obtained 1,261 modules with an average size of 13 nodes. Among the 1,261 PPI modules, 46 encompassed at least one gene identified by the machine learning analysis. We used g:profiler to determine functional enrichment for each module. Cytoscape software [71] was used to visualize the PPI modules.

Genetic risk scores

By optimizing the machine learning-based model, the modified HEAL framework can also make a prediction of disease based on the input genome. We call it rare variant-based genetic risk score (RVS) because it only leverages information on rare variants. Using the trained model, we estimated the RVS prediction performance in the validation cohort. We also analyzed the association between RVS and clinical parameters such as vital signs and blood test data in the BBJ data using Pearson's correlation. To investigate the prognostic impact of RVS, we divided the patients into those in the top 5% and those below, then compared their outcome using Kaplan-Meier analysis and a log-rank test. To compare the properties between RVS and the common variant-based polygenic risk score (PRS), GWAS of CAD in BBJ (case 25,668 vs control 141,667) was performed. The individuals included in the GWAS were genotyped using the HumanOmniExpressExome v.1.0/v.1.2 platform (Illumina) or in combination with HumanOmniExpress v.1.0 and Human Exome BeadChip v.1.0/v.1.1 (Illumina). For genotype quality control, variants with (1) SNP call rate < 99%, (2) Hardy–Weinberg equilibrium ($P < 1 * 10^{-6}$) and (3) heterozygous counts <5 were excluded. We performed pre-phasing using Eagle software. Phased haplotypes were imputed to the in-house reference panel from BBJ [11] by minimac3 [72]. Variants with low

745 imputation quality (R^2<0.3) were excluded. GWAS was performed by logistic
746 regression implemented in PLINK 2.0 [60] with adjustment for age, age^2, sex and first 10
747 principal components of ancestry. Then PRS of *i*th sample was calculated as follows

$$PRS_i = \sum_{j=1}^{M} a_{i,j}\, \beta_j$$

748 , where M is the number of variants in GWAS, $a_{i,j}$ is the number of effect allele of *j*th
749 variant in *i*th sample, and β_j is the effect size of *j*th variant estimated by GWAS. The
750 number of variants included in the PRS calculation was determined by the pruning and
751 thresholding method [13]. The relationship between RVS and PRS was examined by
752 Pearson's correlation coefficient, both in cases only and across the validation cohort. We
753 then integrated both RVS and PRS by normalizing (mean 0, standard deviation 1) and
754 adding them together to obtain combined risk score (CRS). The predictive performance
755 of each genetic score was estimated on the validation cohort, which was not used in the
756 derivation of the RVS, PRS, or CRS. We used receiver operating characteristics (ROC)
757 to evaluate the predictive performance. To examine whether CRS improves predictive
758 performance compared to conventional PRS, we compared AUROC of PRS and CRS
759 by DeLong's test. We also calculated the area under precision-recall curve (AUPRC)
760 and Nagelkerke's pseudo R^2 metrics. The P values were derived using a 20000 times
761 bootstrap replication method. In all statistical analyses, R software was used and a two-
762 sided $P < 0.05$ was considered statistically significant.
763
764

Reference

1. Wang, H., Naghavi, M., Allen, C., Barber, R.M., Bhutta, Z.A., Carter, A., Casey, D.C., Charlson, F.J., Chen, A.Z., Coates, M.M., et al. (2016). Global, regional, and national life expectancy, all-cause mortality, and cause-specific mortality for 249 causes of death, 1980–2015: a systematic analysis for the Global Burden of Disease Study 2015. Lancet *388*, 1459–1544.

2. Roth, G.A., Huffman, M.D., Moran, A.E., Feigin, V., Mensah, G.A., Naghavi, M., and Murray, C.J.L. (2015). Global and regional patterns in cardiovascular mortality from 1990 to 2013. Circulation *132*, 1667–1678.

3. McPherson, R., and Tybjaerg-Hansen, A. (2016). Genetics of Coronary Artery Disease. Circ. Res. *118*, 564–578.

4. Musunuru, K., and Kathiresan, S. (2019). Genetics of Common, Complex Coronary Artery Disease. Cell *177*, 132–145.

5. Khera, A.V., and Kathiresan, S. (2017). Genetics of coronary artery disease: discovery, biology and clinical translation. Nat. Rev. Genet. *18*, 331–344.

6. Marenberg, M.E., Risch, N., Berkman, L.F., Floderus, B., and de Faire, U. (1994). Genetic Susceptibility to Death from Coronary Heart Disease in a Study of Twins. N. Engl. J. Med. *330*, 1041–1046.

7. Zdravkovic, S., Wienke, A., Pedersen, N.L., Marenberg, M.E., Yashin, A.I., and De Faire, U. (2002). Heritability of death from coronary heart disease: a 36-year follow-up of 20 966 Swedish twins. J. Intern. Med. *252*, 247–254.

8. Nikpay, M., Goel, A., Won, H.-H., Hall, L.M., Willenborg, C., Kanoni, S., Saleheen, D., Kyriakou, T., Nelson, C.P., Hopewell, J.C., et al. (2015). A comprehensive 1,000 Genomes-based genome-wide association meta-analysis of coronary artery disease. Nat. Genet. *47*, 1121–1130.

9. van der Harst, P., and Verweij, N. (2018). Identification of 64 Novel Genetic Loci Provides an Expanded View on the Genetic Architecture of Coronary Artery Disease. Circ. Res. *122*, 433–443.

10. Matsunaga, H., Ito, K., Akiyama, M., Takahashi, A., Koyama, S., Nomura, S., Ieki, H., Ozaki, K., Onouchi, Y., Sakaue, S., et al. (2020). Transethnic Meta-Analysis of Genome-Wide Association Studies Identifies Three New Loci and Characterizes Population-Specific Differences for Coronary Artery Disease. Circulation: Genomic and Precision Medicine *13*, e002670.

11. Koyama, S., Ito, K., Terao, C., Akiyama, M., Horikoshi, M., Momozawa, Y., Matsunaga, H., Ieki, H., Ozaki, K., Onouchi, Y., et al. (2020). Population-specific and trans-ancestry genome-wide analyses identify distinct and shared genetic risk loci for coronary artery disease. Nat. Genet. *52*, 1169–1177.

12. Schnitzler, G.R., Kang, H., Fang, S., Angom, R.S., Lee-Kim, V.S., Ma, X.R., Zhou, R., Zeng, T., Guo, K., Taylor, M.S., et al. (2024). Convergence of coronary artery disease genes onto endothelial cell programs. Nature *626*, 799–807.

13. Khera, A.V., Chaffin, M., Aragam, K.G., Haas, M.E., Roselli, C., Choi, S.H., Natarajan, P., Lander, E.S., Lubitz, S.A., Ellinor, P.T., et al. (2018). Genome-wide polygenic scores for common diseases identify individuals with risk equivalent to monogenic mutations. Nat. Genet. *50*, 1219–1224.

14. Torkamani, A., Wineinger, N.E., and Topol, E.J. (2018). The personal and clinical utility of polygenic risk scores. Nat. Rev. Genet. *19*, 581–590.

15. Richardson, T.G., Harrison, S., Hemani, G., and Davey Smith, G. (2019). An atlas of polygenic risk score associations to highlight putative causal relationships across the human phenome. Elife *8*. 10.7554/eLife.43657.

16. Minikel, E.V., Karczewski, K.J., Martin, H.C., Cummings, B.B., Whiffin, N., Rhodes, D., Alföldi, J., Trembath, R.C., van Heel, D.A., Daly, M.J., et al. (2020). Evaluating drug targets through human loss-of-function genetic variation. Nature *581*, 459–464.

17. Backman, J.D., Li, A.H., Marcketta, A., Sun, D., Mbatchou, J., Kessler, M.D., Benner, C., Liu, D., Locke, A.E., Balasubramanian, S., et al. (2021). Exome sequencing and analysis of 454,787 UK Biobank participants. Nature *599*, 628–634.

18. Jurgens, S.J., Choi, S.H., Morrill, V.N., Chaffin, M., Pirruccello, J.P., Halford, J.L., Weng, L.-C., Nauffal, V., Roselli, C., Hall, A.W., et al. (2022). Analysis of rare genetic variation underlying cardiometabolic diseases and traits among 200,000 individuals in the UK Biobank. Nat. Genet. *54*, 240–250.

19. Li, J., Pan, C., Zhang, S., Spin, J.M., Deng, A., Leung, L.L.K., Dalman, R.L., Tsao, P.S., and Snyder, M. (2018). Decoding the Genomics of Abdominal Aortic Aneurysm. Cell *174*, 1361-1372.e10.

20. Do, R., Stitziel, N.O., Won, H.-H., Jørgensen, A.B., Duga, S., Angelica Merlini, P., Kiezun, A., Farrall, M., Goel, A., Zuk, O., et al. (2015). Exome sequencing identifies rare LDLR and APOA5 alleles conferring risk for myocardial infarction. Nature *518*, 102–106.

21. Fishilevich, S., Nudel, R., Rappaport, N., Hadar, R., Plaschkes, I., Iny Stein, T., Rosen, N., Kohn, A., Twik, M., Safran, M., et al. (2017). GeneHancer: genome-wide integration of enhancers and target genes in GeneCards. Database *2017*. 10.1093/database/bax028.

22. Groza, T., Gomez, F.L., Mashhadi, H.H., Muñoz-Fuentes, V., Gunes, O., Wilson, R., Cacheiro, P., Frost, A., Keskivali-Bond, P., Vardal, B., et al. (2023). The International Mouse Phenotyping Consortium: comprehensive knockout

phenotyping underpinning the study of human disease. Nucleic Acids Res. *51*, D1038–D1045.

23. Iacocca, M.A., Chora, J.R., Carrié, A., Freiberger, T., Leigh, S.E., Defesche, J.C., Kurtz, C.L., DiStefano, M.T., Santos, R.D., Humphries, S.E., et al. (2018). ClinVar database of global familial hypercholesterolemia-associated DNA variants. Hum. Mutat. *39*, 1631–1640.

24. Versmissen, J., Oosterveer, D.M., Yazdanpanah, M., Dehghan, A., Hólm, H., Erdman, J., Aulchenko, Y.S., Thorleifsson, G., Schunkert, H., Huijgen, R., et al. (2015). Identifying genetic risk variants for coronary heart disease in familial hypercholesterolemia: an extreme genetics approach. Eur. J. Hum. Genet. *23*, 381–387.

25. Tajima, T., Morita, H., Ito, K., Yamazaki, T., Kubo, M., Komuro, I., and Momozawa, Y. (2018). Blood lipid-related low-frequency variants in LDLR and PCSK9 are associated with onset age and risk of myocardial infarction in Japanese. Sci. Rep. *8*, 1–9.

26. Dickinson, M.E., Flenniken, A.M., Ji, X., Teboul, L., Wong, M.D., White, J.K., Meehan, T.F., Weninger, W.J., Westerberg, H., Adissu, H., et al. (2016). High-throughput discovery of novel developmental phenotypes. Nature *537*, 508–514.

27. Huang, J., Huffman, J.E., Huang, Y., Do Valle, Í., Assimes, T.L., Raghavan, S., Voight, B.F., Liu, C., Barabási, A.-L., Huang, R.D.L., et al. (2022). Genomics and phenomics of body mass index reveals a complex disease network. Nat. Commun. *13*, 7973.

28. Zhu, Z., Guo, Y., Shi, H., Liu, C.-L., Panganiban, R.A., Chung, W., O'Connor, L.J., Himes, B.E., Gazal, S., Hasegawa, K., et al. (2020). Shared genetic and experimental links between obesity-related traits and asthma subtypes in UK Biobank. J. Allergy Clin. Immunol. *145*, 537–549.

29. Liu, M., Jiang, Y., Wedow, R., Li, Y., Brazel, D.M., Chen, F., Datta, G., Davila-Velderrain, J., McGuire, D., Tian, C., et al. (2019). Association studies of up to 1.2 million individuals yield new insights into the genetic etiology of tobacco and alcohol use. Nat. Genet. *51*, 237–244.

30. Cecil, J.E., Tavendale, R., Watt, P., Hetherington, M.M., and Palmer, C.N.A. (2008). An Obesity-Associated FTO Gene Variant and Increased Energy Intake in Children. N. Engl. J. Med. *359*, 2558–2566.

31. Claussnitzer, M., Dankel, S.N., Kim, K.-H., Quon, G., Meuleman, W., Haugen, C., Glunk, V., Sousa, I.S., Beaudry, J.L., Puviindran, V., et al. (2015). FTO Obesity Variant Circuitry and Adipocyte Browning in Humans. N. Engl. J. Med. *373*, 895–907.

32. Locke, A.E., Kahali, B., Berndt, S.I., Justice, A.E., Pers, T.H., Day, F.R., Powell, C.,

878 Vedantam, S., Buchkovich, M.L., Yang, J., et al. (2015). Genetic studies of body
879 mass index yield new insights for obesity biology. Nature *518*, 197–206.

880 33. Richardson, T.G., Sanderson, E., Palmer, T.M., Ala-Korpela, M., Ference, B.A.,
881 Davey Smith, G., and Holmes, M.V. (2020). Evaluating the relationship between
882 circulating lipoprotein lipids and apolipoproteins with risk of coronary heart
883 disease: A multivariable Mendelian randomisation analysis. PLoS Med. *17*,
884 e1003062.

885 34. Sakaue, S., Kanai, M., Tanigawa, Y., Karjalainen, J., Kurki, M., Koshiba, S., Narita,
886 A., Konuma, T., Yamamoto, K., Akiyama, M., et al. (2021). A cross-population
887 atlas of genetic associations for 220 human phenotypes. Nat. Genet. *53*, 1415–
888 1424.

889 35. Zhuang, Z., Yao, M., Wong, J.Y.Y., Liu, Z., and Huang, T. (2021). Shared genetic
890 etiology and causality between body fat percentage and cardiovascular diseases: a
891 large-scale genome-wide cross-trait analysis. BMC Med. *19*, 100.

892 36. Evangelou, E., Warren, H.R., Mosen-Ansorena, D., Mifsud, B., Pazoki, R., Gao, H.,
893 Ntritsos, G., Dimou, N., Cabrera, C.P., Karaman, I., et al. (2018). Genetic analysis
894 of over 1 million people identifies 535 new loci associated with blood pressure
895 traits. Nat. Genet. *50*, 1412–1425.

896 37. Sinnott-Armstrong, N., Tanigawa, Y., Amar, D., Mars, N., Benner, C., Aguirre, M.,
897 Venkataraman, G.R., Wainberg, M., Ollila, H.M., Kiiskinen, T., et al. (2021).
898 Genetics of 35 blood and urine biomarkers in the UK Biobank. Nat. Genet. *53*,
899 185–194.

900 38. Gargano, M.A., Matentzoglu, N., Coleman, B., Addo-Lartey, E.B.,
901 Anagnostopoulos, A.V., Anderton, J., Avillach, P., Bagley, A.M., Bakštein, E.,
902 Balhoff, J.P., et al. (2024). The Human Phenotype Ontology in 2024: phenotypes
903 around the world. Nucleic Acids Res. *52*, D1333–D1346.

904 39. Nordestgaard, B.G., Nicholls, S.J., Langsted, A., Ray, K.K., and Tybjærg-Hansen,
905 A. (2018). Advances in lipid-lowering therapy through gene-silencing technologies.
906 Nat. Rev. Cardiol. *15*, 261–272.

907 40. Raal, F.J., Rosenson, R.S., Reeskamp, L.F., Hovingh, G.K., Kastelein, J.J.P., Rubba,
908 P., Ali, S., Banerjee, P., Chan, K.-C., Gipe, D.A., et al. (2020). Evinacumab for
909 Homozygous Familial Hypercholesterolemia. N. Engl. J. Med. *383*, 711–720.

910 41. Kessler, T., and Schunkert, H. (2021). Coronary Artery Disease Genetics
911 Enlightened by Genome-Wide Association Studies. JACC Basic Transl Sci *6*, 610–
912 623.

913 42. Mortensen, M.B., and Nordestgaard, B.G. (2020). Elevated LDL cholesterol and
914 increased risk of myocardial infarction and atherosclerotic cardiovascular disease
915 in individuals aged 70–100 years: a contemporary primary prevention cohort.

Lancet *396*, 1644–1652.

43. Howard, B.V., Robbins, D.C., Sievers, M.L., Lee, E.T., Rhoades, D., Devereux, R.B., Cowan, L.D., Gray, R.S., Welty, T.K., Go, O.T., et al. (2000). LDL cholesterol as a strong predictor of coronary heart disease in diabetic individuals with insulin resistance and low LDL: The Strong Heart Study. Arterioscler. Thromb. Vasc. Biol. *20*, 830–835.

44. Zhao, J.V., and Schooling, C.M. (2018). Coagulation Factors and the Risk of Ischemic Heart Disease. Circulation: Genomic and Precision Medicine *11*, e001956.

45. Ndrepepa, G., and Kastrati, A. (2019). Alanine aminotransferase—a marker of cardiovascular risk at high and low activity levels. J. Lab. Precis. Med. *4*, 29–29.

46. Shen, H., Zeng, C., Wu, X., Liu, S., and Chen, X. (2019). Prognostic value of total bilirubin in patients with acute myocardial infarction: A meta-analysis. Medicine *98*, e13920.

47. Emerging Risk Factors Collaboration, Di Angelantonio, E., Sarwar, N., Perry, P., Kaptoge, S., Ray, K.K., Thompson, A., Wood, A.M., Lewington, S., Sattar, N., et al. (2009). Major lipids, apolipoproteins, and risk of vascular disease. JAMA *302*, 1993–2000.

48. Auer, P.L., and Lettre, G. (2015). Rare variant association studies: considerations, challenges and opportunities. Genome Med. *7*, 16.

49. Chen, W., Coombes, B.J., and Larson, N.B. (2022). Recent advances and challenges of rare variant association analysis in the biobank sequencing era. Front. Genet. *13*, 1014947.

50. Khetarpal, S.A., Babb, P.L., Zhao, W., Hancock-Cerutti, W.F., Brown, C.D., Rader, D.J., and Voight, B.F. (2018). Multiplexed Targeted Resequencing Identifies Coding and Regulatory Variation Underlying Phenotypic Extremes of High-Density Lipoprotein Cholesterol in Humans. Circ Genom Precis Med *11*, e002070.

51. Diaz-Uriarte, R., Gómez de Lope, E., Giugno, R., Fröhlich, H., Nazarov, P.V., Nepomuceno-Chamorro, I.A., Rauschenberger, A., and Glaab, E. (2022). Ten quick tips for biomarker discovery and validation analyses using machine learning. PLoS Comput. Biol. *18*, e1010357.

52. Fahed, A.C., Wang, M., Homburger, J.R., Patel, A.P., Bick, A.G., Neben, C.L., Lai, C., Brockman, D., Philippakis, A., Ellinor, P.T., et al. (2020). Polygenic background modifies penetrance of monogenic variants for tier 1 genomic conditions. Nat. Commun. *11*, 3635.

53. Chen, Z., and Schunkert, H. (2021). Genetics of coronary artery disease in the post-GWAS era. J. Intern. Med. *290*, 980–992.

54. Martin, A.R., Kanai, M., Kamatani, Y., Okada, Y., Neale, B.M., and Daly, M.J. (2019). Clinical use of current polygenic risk scores may exacerbate health disparities. Nat. Genet. *51*, 584–591.

55. Nagai, A., Hirata, M., Kamatani, Y., Muto, K., Matsuda, K., Kiyohara, Y., Ninomiya, T., Tamakoshi, A., Yamagata, Z., Mushiroda, T., et al. (2017). Overview of the BioBank Japan Project: Study design and profile. J. Epidemiol. *27*, S2–S8.

56. Hirata, M., Kamatani, Y., Nagai, A., Kiyohara, Y., Ninomiya, T., Tamakoshi, A., Yamagata, Z., Kubo, M., Muto, K., Mushiroda, T., et al. (2017). Cross-sectional analysis of BioBank Japan clinical data: A large cohort of 200,000 patients with 47 common diseases. J. Epidemiol. *27*, S9–S21.

57. Setoh, K., and Matsuda, F. (2022). Cohort Profile: The Nagahama Prospective Genome Cohort for Comprehensive Human Bioscience (The Nagahama Study). In Socio-Life Science and the COVID-19 Outbreak: Public Health and Public Policy, M. Yano, F. Matsuda, A. Sakuntabhai, and S. Hirota, eds. (Springer Singapore), pp. 127–143.

58. Li, H., and Durbin, R. (2009). Fast and accurate short read alignment with Burrows-Wheeler transform. Bioinformatics *25*, 1754–1760.

59. Galinsky, K.J., Bhatia, G., Loh, P.-R., Georgiev, S., Mukherjee, S., Patterson, N.J., and Price, A.L. (2016). Fast Principal-Component Analysis Reveals Convergent Evolution of ADH1B in Europe and East Asia. Am. J. Hum. Genet. *98*, 456–472.

60. Chang, C.C., Chow, C.C., Tellier, L.C., Vattikuti, S., Purcell, S.M., and Lee, J.J. (2015). Second-generation PLINK: rising to the challenge of larger and richer datasets. Gigascience *4*, 7.

61. Price, A.L., Patterson, N.J., Plenge, R.M., Weinblatt, M.E., Shadick, N.A., and Reich, D. (2006). Principal components analysis corrects for stratification in genome-wide association studies. Nat. Genet. *38*, 904–909.

62. Zhou, W., Nielsen, J.B., Fritsche, L.G., Dey, R., Gabrielsen, M.E., Wolford, B.N., LeFaive, J., VandeHaar, P., Gagliano, S.A., Gifford, A., et al. (2018). Efficiently controlling for case-control imbalance and sample relatedness in large-scale genetic association studies. Nat. Genet. *50*, 1335–1341.

63. Zhou, W., Zhao, Z., Nielsen, J.B., Fritsche, L.G., LeFaive, J., Gagliano Taliun, S.A., Bi, W., Gabrielsen, M.E., Daly, M.J., Neale, B.M., et al. (2020). Scalable generalized linear mixed model for region-based association tests in large biobanks and cohorts. Nat. Genet. *52*, 634–639.

64. Zhou, W., Bi, W., Zhao, Z., Dey, K.K., Jagadeesh, K.A., Karczewski, K.J., Daly, M.J., Neale, B.M., and Lee, S. (2021). Set-based rare variant association tests for biobank scale sequencing data sets. medRxiv, 2021.07.12.21260400.

65. Ioannidis, N.M., Rothstein, J.H., Pejaver, V., Middha, S., McDonnell, S.K., Baheti,

S., Musolf, A., Li, Q., Holzinger, E., Karyadi, D., et al. (2016). REVEL: An Ensemble Method for Predicting the Pathogenicity of Rare Missense Variants. Am. J. Hum. Genet. *99*, 877–885.

66. Wang, K., Li, M., and Hakonarson, H. (2010). ANNOVAR: functional annotation of genetic variants from high-throughput sequencing data. Nucleic Acids Res. *38*, e164.

67. A global reference for human genetic variation | Nature https://www.nature.com › articleshttps://www.nature.com › articles.

68. Karczewski, K.J., Francioli, L.C., Tiao, G., Cummings, B.B., Alföldi, J., Wang, Q., Collins, R.L., Laricchia, K.M., Ganna, A., Birnbaum, D.P., et al. (2020). The mutational constraint spectrum quantified from variation in 141,456 humans. Nature *581*, 434–443.

69. Kolberg, L., Raudvere, U., Kuzmin, I., Adler, P., Vilo, J., and Peterson, H. (2023). g:Profiler-interoperable web service for functional enrichment analysis and gene identifier mapping (2023 update). Nucleic Acids Res. *51*, W207–W212.

70. Blondel, V.D., Guillaume, J.-L., Lambiotte, R., and Lefebvre, E. (2008). Fast unfolding of communities in large networks. J. Stat. Mech. *2008*, P10008.

71. Shannon, P., Markiel, A., Ozier, O., Baliga, N.S., Wang, J.T., Ramage, D., Amin, N., Schwikowski, B., and Ideker, T. (2003). Cytoscape: a software environment for integrated models of biomolecular interaction networks. Genome Res. *13*, 2498–2504.

72. Das, S., Forer, L., Schönherr, S., Sidore, C., Locke, A.E., Kwong, A., Vrieze, S.I., Chew, E.Y., Levy, S., McGue, M., et al. (2016). Next-generation genotype imputation service and methods. Nat. Genet. *48*, 1284–1287.

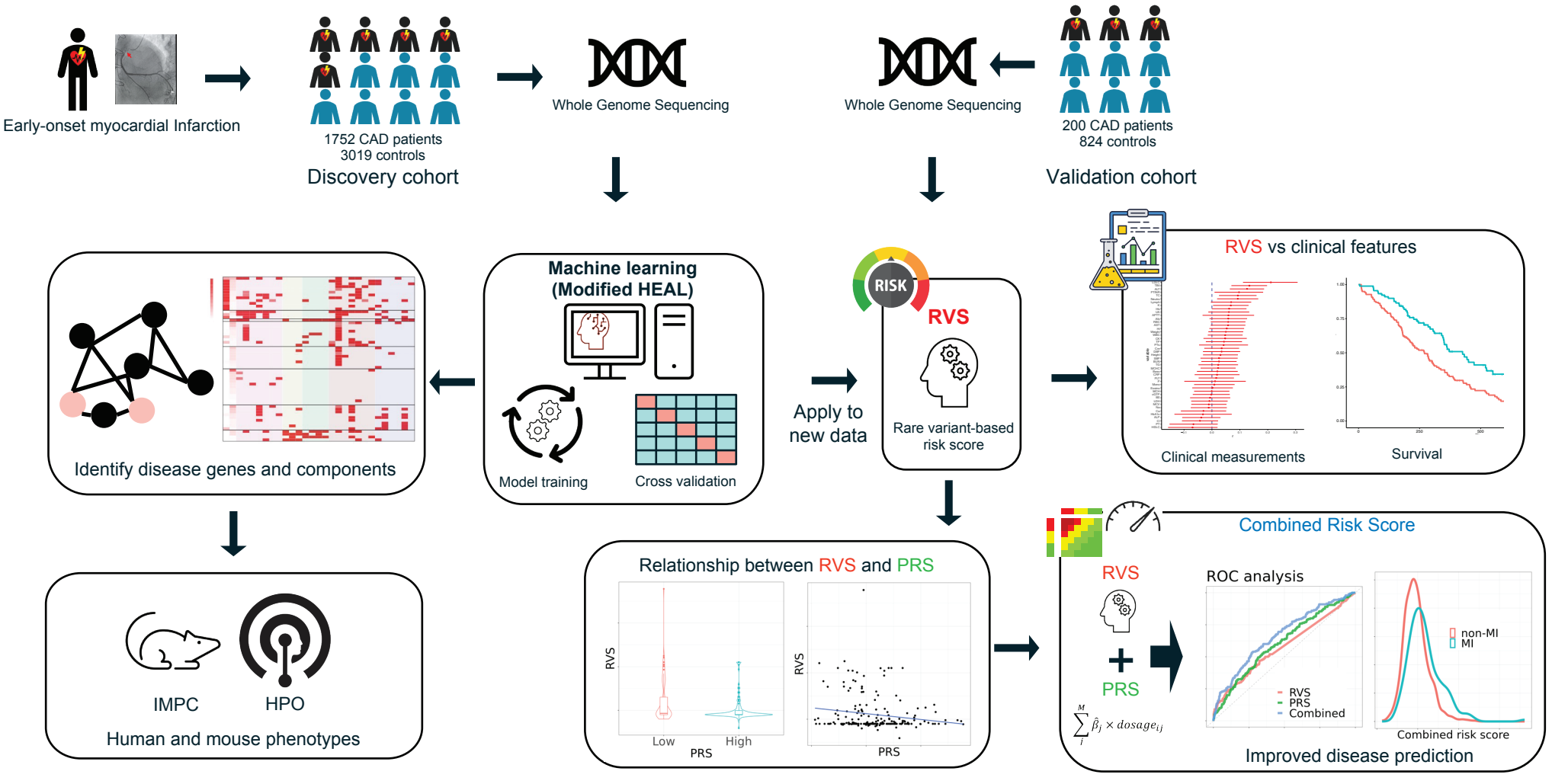
Early-onset myocardial Infarction
1752 CAD patients
3019 controls
Discovery cohort
Whole Genome Sequencing
Whole Genome Sequencing
200 CAD patients
824 controls
Validation cohort
Machine learning
(Modified HEAL)
Model training
Cross validation
Identify disease genes and components
IMPC
HPO
Human and mouse phenotypes
Apply to
new data
RISK
RVS
Rare variant-based
risk score
RVS vs clinical features
Clinical measurements
Survival
Relationship between RVS and PRS
RVS
PRS
Low
High
Combined Risk Score
RVS
PRS
ROC analysis
RVS
PRS
Combined
non-MI
MI
Combined risk score
Improved disease prediction

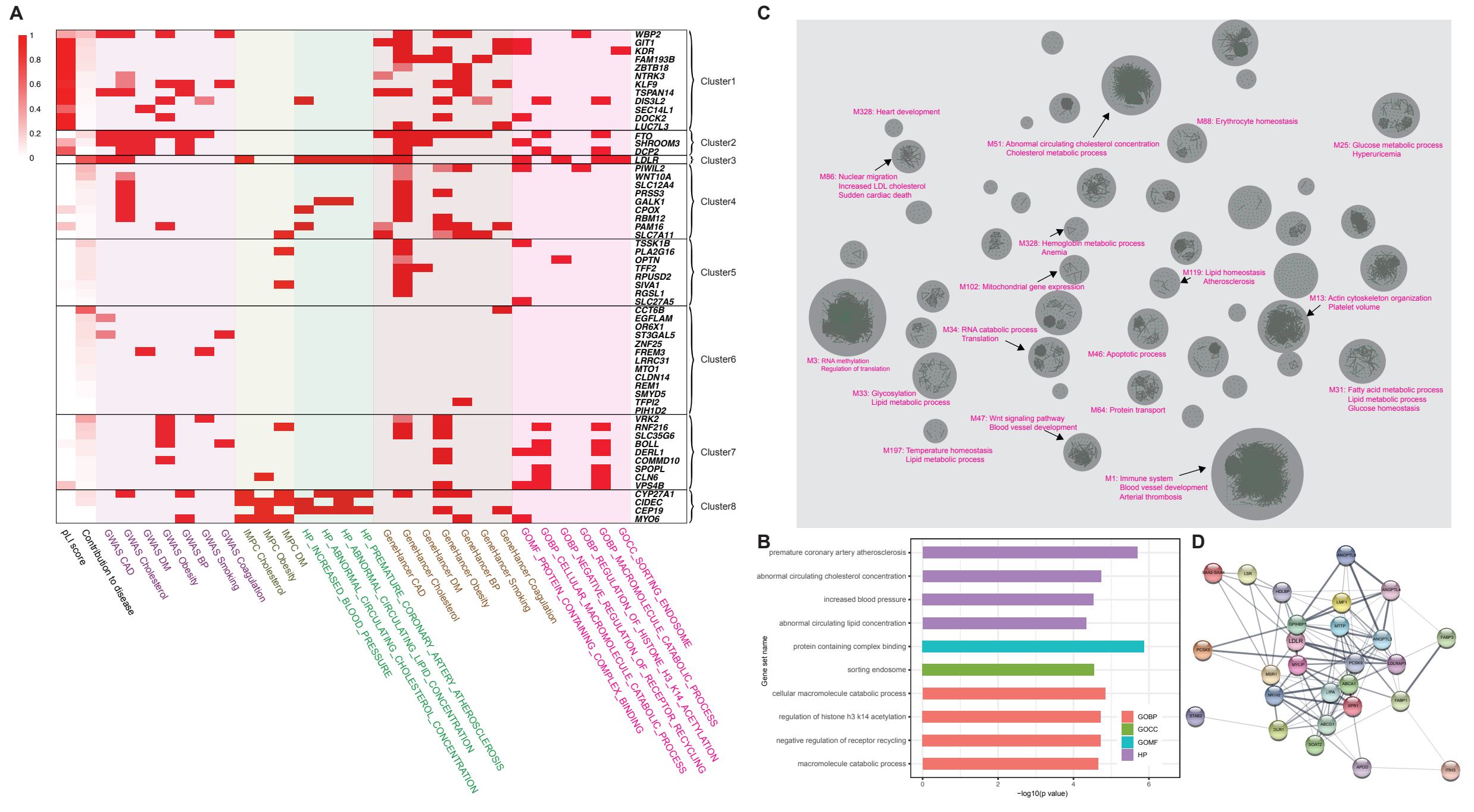
A
1
0.8
0.6
0.4
0.2
0
WBP2
GIT1
KDR
FAM193B
ZBTB18
NTRK3
KLF9
TSPAN14
DIS3L2
SEC14L1
DOCK2
LUC7L3
FTO
SHROOM3
DCP2
LDLR
PIWIL2
WNT10A
SLC12A4
PRSS3
GALK1
CPOX
RBM12
PAM16
SLC7A11
TSSK1B
PLA2G16
OPTN
TFF2
RPUSD2
SIVA1
RGSL1
SLC27A5
CCT6B
EGFLAM
OR6X1
ST3GAL5
ZNF25
FREM3
LRRC31
MTO1
CLDN14
REM1
SMYD5
TFPI2
PIH1D2
VRK2
RNF216
SLC35G6
BOLL
DERL1
COMMD10
SPOPL
CLN6
VPS4B
CYP27A1
CIDEC
CEP19
MYO6
Cluster1
Cluster2
Cluster3
Cluster4
Cluster5
Cluster6
Cluster7
Cluster8
pLI score
Contribution to disease
GWAS CAD
GWAS Cholesterol
GWAS DM
GWAS Obesity
GWAS BP
GWAS Smoking
GWAS Coagulation
IMPC Cholesterol
IMPC Obesity
IMPC DM
HP_INCREASED_BLOOD_PRESSURE
HP_ABNORMAL_CIRCULATING_CHOLESTEROL_CONCENTRATION
HP_ABNORMAL_CIRCULATING_LIPID_CONCENTRATION
HP_PREMATURE_CORONARY_ARTERY_ATHEROSCLEROSIS
GeneHancer CAD
GeneHancer Cholesterol
GeneHancer DM
GeneHancer Obesity
GeneHancer BP
GeneHancer Smoking
GeneHancer Coagulation
GOMF_PROTEIN_CONTAINING_COMPLEX_BINDING
GOBP_CELLULAR_MACROMOLECULE_CATABOLIC_PROCESS
GOBP_NEGATIVE_REGULATION_OF_HISTONE_H3_K14_ACETYLATION
GOBP_REGULATION_OF_RECEPTOR_RECYCLING
GOBP_MACROMOLECULE_CATABOLIC_PROCESS
GOCC_SORTING_ENDOSOME
C
M328: Heart development
M86: Nuclear migration
Increased LDL cholesterol
Sudden cardiac death
M51: Abnormal circulating cholesterol concentration
Cholesterol metabolic process
M88: Erythrocyte homeostasis
M25: Glucose metabolic process
Hyperuricemia
M328: Hemoglobin metabolic process
Anemia
M102: Mitochondrial gene expression
M119: Lipid homeostasis
Atherosclerosis
M13: Actin cytoskeleton organization
Platelet volume
M34: RNA catabolic process
Translation
M3: RNA methylation
Regulation of translation
M46: Apoptotic process
M33: Glycosylation
Lipid metabolic process
M64: Protein transport
M31: Fatty acid metabolic process
Lipid metabolic process
Glucose homeostasis
M47: Wnt signaling pathway
Blood vessel development
M197: Temperature homeostasis
Lipid metabolic process
M1: Immune system
Blood vessel development
Arterial thrombosis
B
premature coronary artery atherosclerosis
abnormal circulating cholesterol concentration
increased blood pressure
abnormal circulating lipid concentration
protein containing complex binding
sorting endosome
cellular macromolecule catabolic process
regulation of histone h3 k14 acetylation
negative regulation of receptor recycling
macromolecule catabolic process
Gene set name
GOBP
GOCC
GOMF
HP
0
2
4
6
−log10(p value)
D
SAA2-SAA4
LSR
HDLBP
ANGPTL3
ANGPTL4
LMF1
GPIHBP1
MTTP
LDLR
FABP3
PCSK9
MYLIP
LDLRAP1
MSR1
ABCA1
NR1H2
LIPA
XPR1
FABP1
STAB1
DLR1
ABCG1
SOAT2
APOD
ITIH3

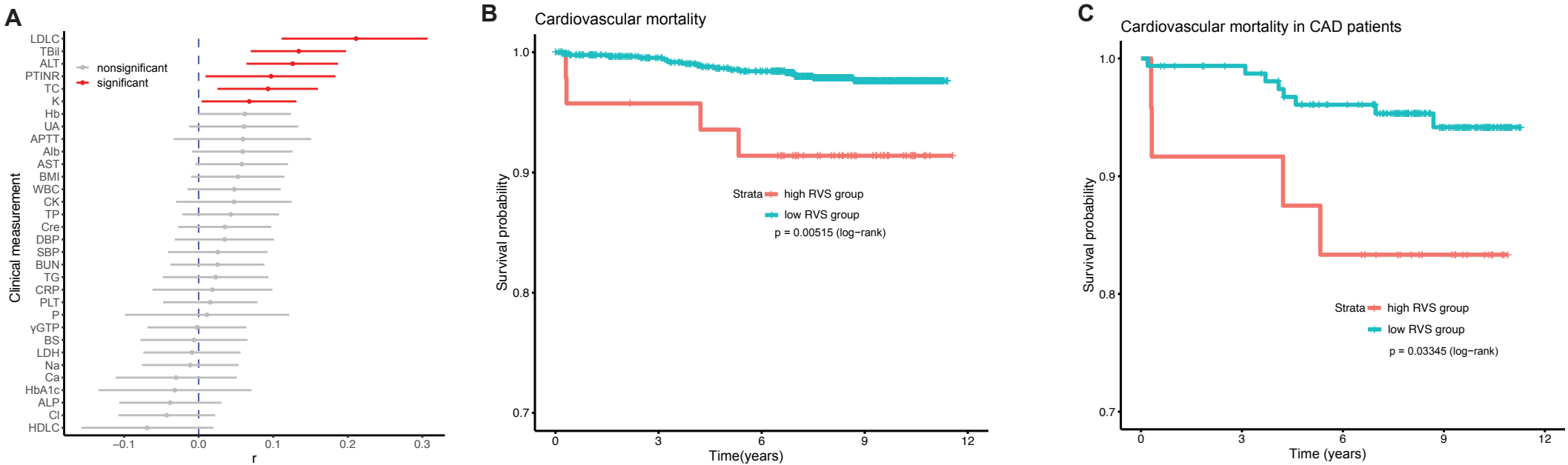
A
LDLC
TBil
ALT
PTINR
TC
K
Hb
UA
APTT
Alb
AST
BMI
WBC
CK
TP
Cre
DBP
SBP
BUN
TG
CRP
PLT
P
γGTP
BS
LDH
Na
Ca
HbA1c
ALP
Cl
HDLC
nonsignificant
significant
Clinical measurement
−0.1
0.0
0.1
0.2
0.3
r
B
Cardiovascular mortality
Survival probability
1.0
0.9
0.8
0.7
Strata
high RVS group
low RVS group
p = 0.00515 (log−rank)
0
3
6
9
12
Time(years)
C
Cardiovascular mortality in CAD patients
Survival probability
1.0
0.9
0.8
0.7
Strata
high RVS group
low RVS group
p = 0.03345 (log−rank)
0
3
6
9
12
Time (years)

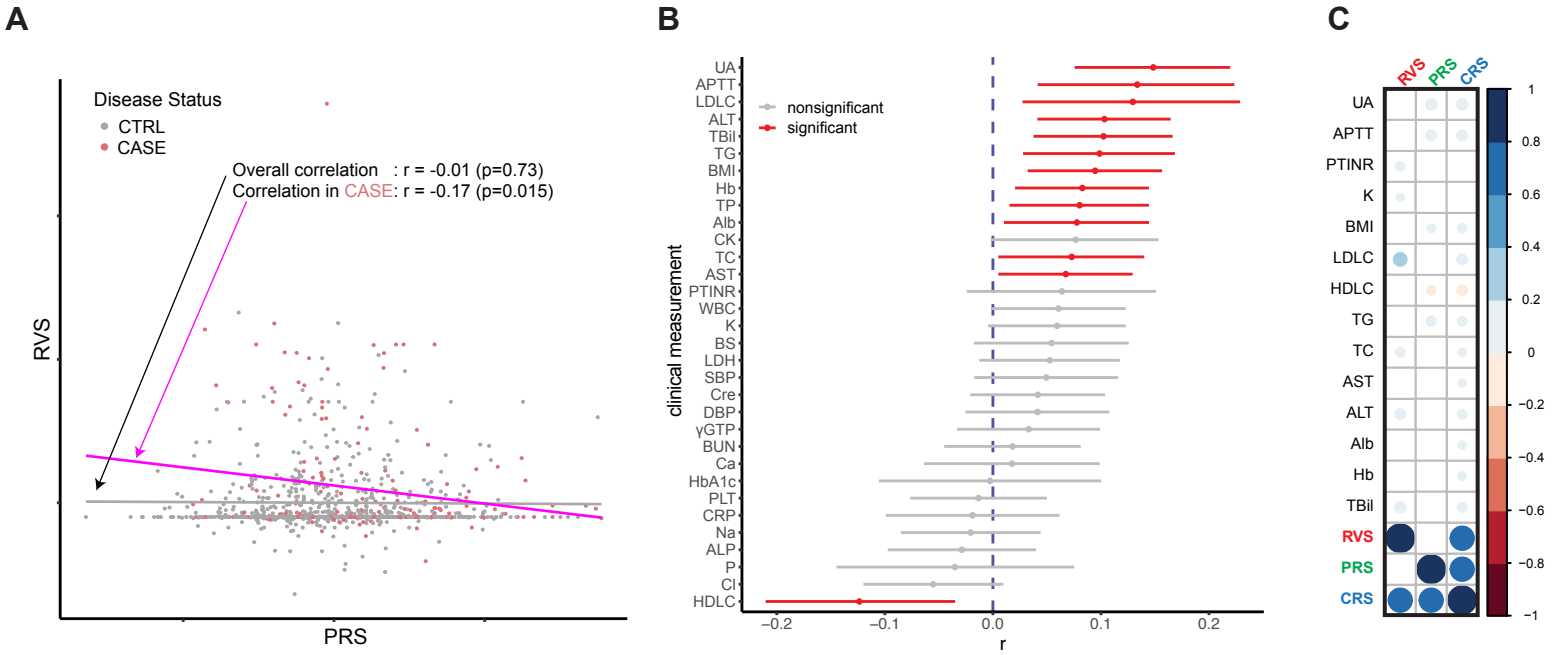
A
Disease Status
CTRL
CASE
Overall correlation : r = -0.01 (p=0.73)
Correlation in CASE: r = -0.17 (p=0.015)
RVS
PRS
B
nonsignificant
significant
clinical measurement
UA
APTT
LDLC
ALT
TBil
TG
BMI
Hb
TP
Alb
CK
TC
AST
PTINR
WBC
K
BS
LDH
SBP
Cre
DBP
γGTP
BUN
Ca
HbA1c
PLT
CRP
Na
ALP
P
Cl
HDLC
−0.2
−0.1
0.0
0.1
0.2
r
C
RVS
PRS
CRS
UA
APTT
PTINR
K
BMI
LDLC
HDLC
TG
TC
AST
ALT
Alb
Hb
TBil
RVS
PRS
CRS
1
0.8
0.6
0.4
0.2
0
−0.2
−0.4
−0.6
−0.8
−1

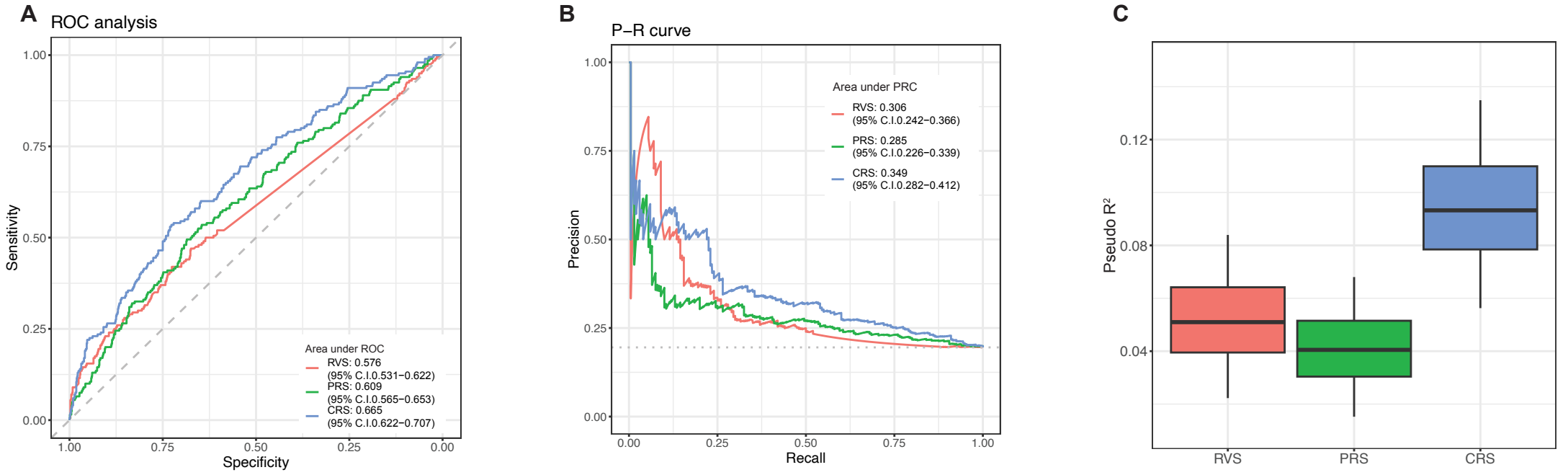
A
ROC analysis
Sensitivity
Specificity
1.00
0.75
0.50
0.25
0.00
Area under ROC
RVS: 0.576
(95% C.I.0.531−0.622)
PRS: 0.609
(95% C.I.0.565−0.653)
CRS: 0.665
(95% C.I.0.622−0.707)
B
P−R curve
Precision
Recall
Area under PRC
RVS: 0.306
(95% C.I.0.242−0.366)
PRS: 0.285
(95% C.I.0.226−0.339)
CRS: 0.349
(95% C.I.0.282−0.412)
C
Pseudo R²
0.12
0.08
0.04
RVS
PRS
CRS